Modeling With RTS Noise Characterization of Novel Embedded Photogate Single-Photon Avalanche Diode for Circuit Simulations

Jian Yang, Yang Wang, Xiangliang Jin, *Member, IEEE*, Yan Peng, Jun Luo, and Jun Yang

***Abstract*—Single-photon avalanche diodes (SPADs) are widely used for weak light detection due to their high gain and high sensitivity. Unfortunately, SPAD devices have random telegraph signal (RTS) noise during the avalanche transition phase, which makes circuit design more difficult. Therefore, the modeling of RTS noise in SPAD devices is of great significance for the design of signal processing circuits. However, RTS noise is not included in the traditional equivalent circuit model. In response to the above problems, this paper implements an equivalent circuit model with RTS noise based on the Cadence. The model is built based on the basic components in the library, and it has strong application universality. The model is validated in a novel embedded photogate SPAD device (EP-SPAD). It accurately simulates the RTS noise and IV characteristics of the EP-SPAD device. In addition, the threshold voltage of EP-SPAD device operating in Geiger mode is precisely defined based on the characteristics of RTS noise. When the reverse bias voltage is increased from 0 V to 15 V, the IV characteristics of the model are consistent with the EP-SPAD device.**

***Index Terms*—Silicon nanophotonics, photodetectors, sensors.**

I. Introduction

In THE fields of fluorescence lifetime imaging, quantum communication and laser ranging, the photon detection probability (PDP) and noise performance of photodetectors are very important [1], [2], [3]. Unfortunately, photomultiplier tubes (PMT) operate at high voltages [4]. In addition, the manufacturing process of the PMT is not compatible with the Complementary Metal Oxide Semiconductor (CMOS) process, and it is difficult to integrate with the signal processing circuit. Now, single-photon avalanche diode (SPAD) devices are widely used for weak light detection due to their high gain [5], [6], [7]. It can be integrated with CMOS signal processing circuit, the signal-to-noise ratio (SNR) of the circuit is greatly improved, and the system volume is reduced [8]. Therefore, accurate simulation of the electrical behavior of SPAD devices is beneficial to the design of signal processing circuits [9], [10], [11], [12].

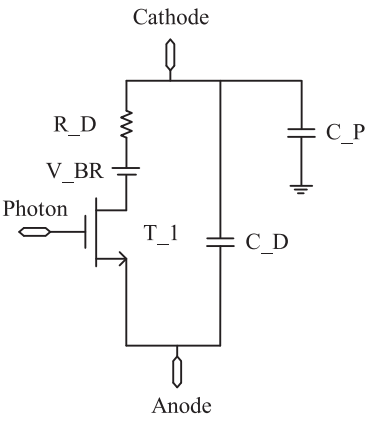

Fig. 1. A simple equivalent circuit model of SPAD device.

Resistor R_D, voltage V_BR and transistor T_1 constitute a simple equivalent circuit model of the SPAD device, as shown in Fig. 1 [13]. V_BR is the avalanche breakdown voltage of the SPAD device. R_D is the equivalent resistance of the device. If the reverse bias voltage is greater than V_BR, the device operates in Geiger mode. The input signal "Photon" is used to simulate photons. When the input signal "Photon" is high voltage, the transistor T_1 is turned on, and the model outputs the avalanche current. This means that the device absorbs photons and generates an avalanche current. When the input signal "Photon" is low voltage, the transistor T_1 is turned off, and the model does not output avalanche current. This means that the device is not receiving photons. This equivalent circuit simulates the triggering and shutdown of the avalanche current for the SPAD device. This provides ideas for model design of SPAD devices. In 2007, Dalla Mora et al. realized an equivalent circuit model for SPAD devices based on Cadence [14]. The model simulates the self-sustaining and self-quenching processes of SPAD devices. In addition, the model characterizes the reverse current-voltage characteristics of SPAD devices. In 2009, F. Zappa et al. implemented equivalent circuit models for SPAD devices in PSpice and Spectre, respectively [15]. This work shows

Manuscript received 23 August 2022; accepted 27 August 2022. Date of publication 31 August 2022; date of current version 13 September 2022. This work was supported in part by the National Natural Science Foundation of China under Grants 62174052 and 61827812, in part by the Hunan Science and Technology Department Huxiang High-level Talent Gathering Project under Grant 2019RS1037, and in part by the Innovation Project of Science and Technology Department of Hunan Province under Grants 2020GK2018 and 2019GK4016. *(Corresponding author: Xiangliang Jin.)*

Jian Yang, Yang Wang, and Xiangliang Jin are with the School of Physics and Electronics, Hunan Normal University, Changsha 410081, China (e-mail: 514625349@qq.com; 365177282@qq.com; jinxl@hunnu.edu.cn).

Yan Peng and Jun Luo are with the School of Mechatronic Engineering and Automation, Shanghai University, Shanghai 200444, China (e-mail: pengpengpy@163.com; luojun@shu.edu.cn).

Jun Yang is with the Institute of Advanced Studies, University of Electronic Science and Technology of China, Shenzhen 518110, China (e-mail: junyang@uestc.edu.cn).

Digital Object Identifier 10.1109/JPHOT.2022.3203046

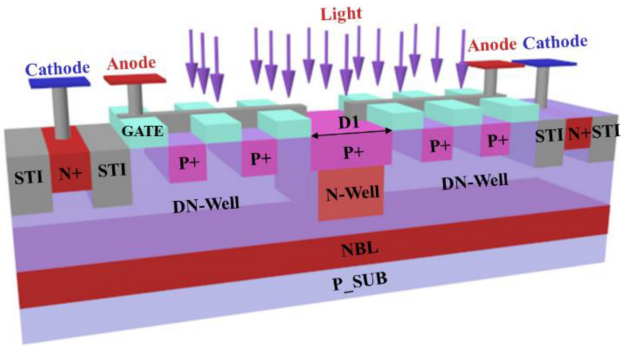

Fig. 2. Structure of the EP-SPAD device.

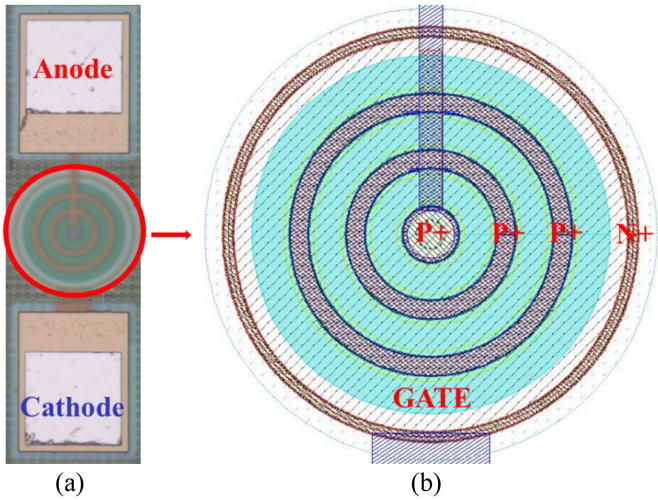

Fig. 3. (a) The layout of the EP-SPAD device. (b) Electron microscope image of the EP-SPAD device.

in detail how to set the parameters of the model based on the experimental results. In addition, the model shows the forward region and secondary breakdown effects. However, these models do not show the reverse current-voltage characteristics of SPAD devices in the linear region. More importantly, RTS noise is not included in these models.

RTS noise exists in the avalanche transition phase of SPAD devices. When the SPAD device is biased near its breakdown voltage, the SPAD device generates avalanche current. At this time, the avalanche current of the device is so small that it is not self-sustaining. Therefore, the avalanche current is self-quenching. The avalanche current of the SPAD device always switches between self-sustaining and self-quenching. This shows the behavior of RTS noise [16], [17], [18]. RTS noise has a negative impact on the performance of SPAD devices, which increases the design difficulty of signal processing circuits [19], [20]. In this paper, a novel embedded photogate SPAD (EP-SPAD) device is fabricated based on a standard silicon-based 0.18 μm BCD process, and the RTS noise of the EP-SPAD device is tested, analyzed, and modeled. The threshold voltage of the EP-SPAD device operating in Geiger mode is precisely defined based on the characteristics of RTS noise. The equivalent circuit model of the EP-SPAD device is built based on Cadence. The model includes RTS noise for the first time. In addition, this paper shows in detail how to calculate the parameters of the model based on the test data. The simulation results show that the model can simulate the behavior of RTS noise, and it accurately characterizes the reverse current-voltage curve of the EP-SPAD device.

II. Principle of The EP-SPAD Device

The structure of EP-SPAD device is shown in Fig. 2. The EP-SPAD device is fabricated based on a standard silicon-based 0.18 μm BCD process. The layout and electron microscope images of the EP-SPAD device are shown in Fig. 3(a) and (b), respectively. The device is based on a photogate and a PN junction formed by P+/N-Well to detect photons. The polysilicon gate and P+ constitute the photogate device. The spectral response range of the EP-SPAD device is extended by the embedded photogate [21]. The avalanche multiplication region is composed of P+/N-Well.

The deep N-well (DN-Well) is used as a dummy guard ring for the device. The diameter of the active area is 12 μm (D1) and the diameter of the polysilicon gate is 8 μm. P+ is connected to the gate, which is the anode of the device. N+/N-Well/DN-Well constitutes the cathode of the device. The avalanche multiplication region and shallow trench isolation (STI) are isolated by the gate-all-around design of the device. This is very important to reduce the dark count rate (DCR) of the EP-SPAD device [22], [23].

The electric field distribution of EP-SPAD device is simulated based on Technology-Computer Aided Design (TCAD) platform. The cathode voltage of EP-SPAD device is set to 12 V, and the anode voltage is set to 0 V. When the reverse bias voltage is greater than the avalanche breakdown voltage, avalanche breakdown occurs in the reverse PN junction formed by P+/N-Well. The electric field in the avalanche multiplication region is very strong. The electric field distribution of the EP-SPAD device is shown in Fig. 4(a). The electric field intensity of the x-cutline is shown in Fig. 4(b). The maximum electric field on the planar PN junction formed by P+/N-Well is about 5.74 $\times$ 10^5 V / cm. The electric field strength of the side junction is about 2×10^5 V/cm, which is much smaller than that of the planar junction. This proves that the DN-Well dummy guard ring prevents edge breakdown. This is the premise of the device working in Geiger mode [24]. When a photon is absorbed by a photogate or a PN junction formed by P+/N-Well, electrons in the valence band absorb the photon energy and then transition to the conduction band to form electron-hole pairs. Electron-hole pairs are accelerated by the strong electric field, and they collide with the lattice to generate new photogenerated carriers. This results in a dramatic increase in the number of photogenerated carriers. Therefore, the output current of the EP-SPAD device is increased, thereby realizing the detection of weak light.

III. Principle of The Equivalent Circuit Model

Compared with Refs. [16], [17], [18], the depletion region of EP-SPAD device is wider. There is a depletion region under the

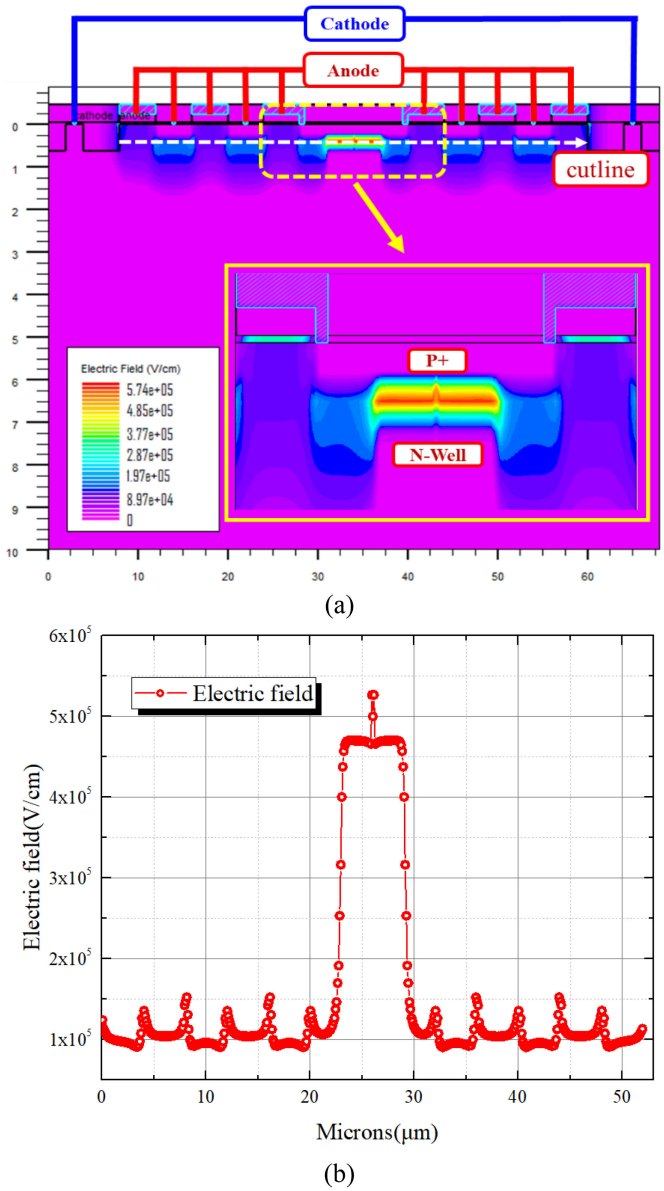

Fig. 4. (a) Electric field distribution of EP-SPAD device. (b) The electric field intensity of the x-cutline.

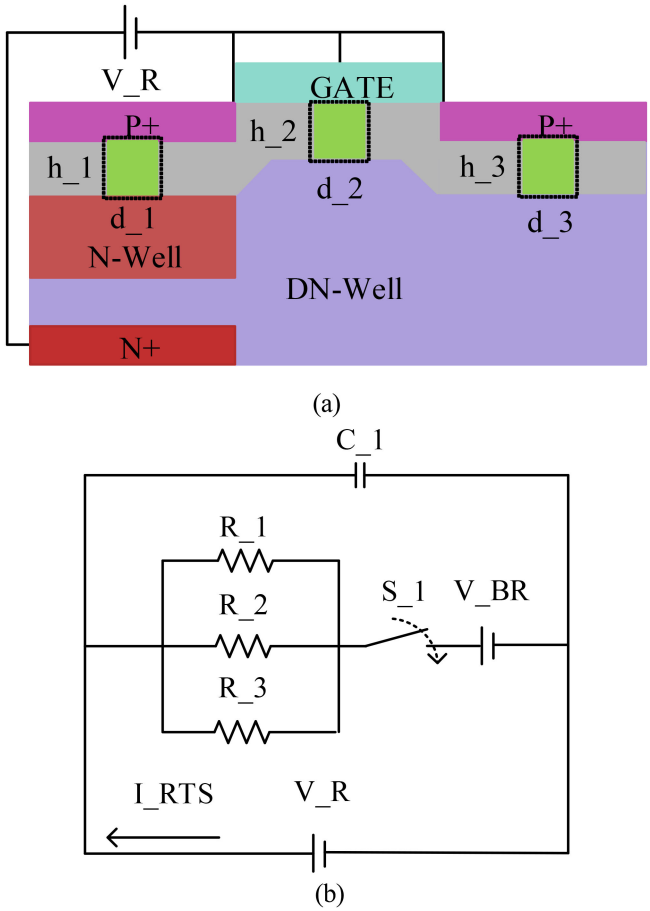

Fig. 5. (a) Defects in the depletion region of the EP-SPAD device. (b) Equivalent circuit model of RTS noise.

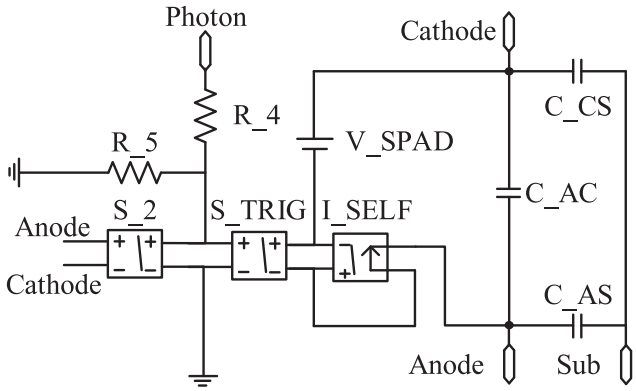

Fig. 6. The traditional equivalent circuit model of SPAD devices.

polysilicon gate, and the PN junction formed by P+/DN-Well also has a depletion region. The defect model of the depletion region in the EP-SPAD device is shown in Fig. 5(a). The heights of the defects are h_1, h_2, and h_3, respectively. The diameters of the defects are d_1, d_2, and d_3, respectively. The equivalent circuit model of RTS noise is shown in Fig. 5(b). The V_R is the reverse bias voltage. This voltage is provided by a Direct Current (DC) regulated power supply. The V_BR is the avalanche breakdown voltage of the EP-SPAD device. The I_RTS is the current of RTS noise. The C_1 is the equivalent capacitance of the device. R_1, R_2 and R_3 are the equivalent resistances of the defects in the three depletion regions, respectively. They mainly depend on the height and diameter of the defects in the depletion region. Switch S_1 is used to simulate RTS noise. When S_1 = 0, switch S_1 is closed and RTS noise is generated in the circuit. The current of RTS noise is I _ RTS. This means that the EP-SPAD device generates avalanche current. When S_1 = 1, switch S_1 is open and there is no RTS noise in the circuit. This means that the EP-SPAD device does not generate avalanche current.

The equivalent circuit model shown in Fig. 6 does not include RTS noise. In this paper, this model is named as the traditional equivalent circuit model [14]. The I_SELF is the self-sustaining

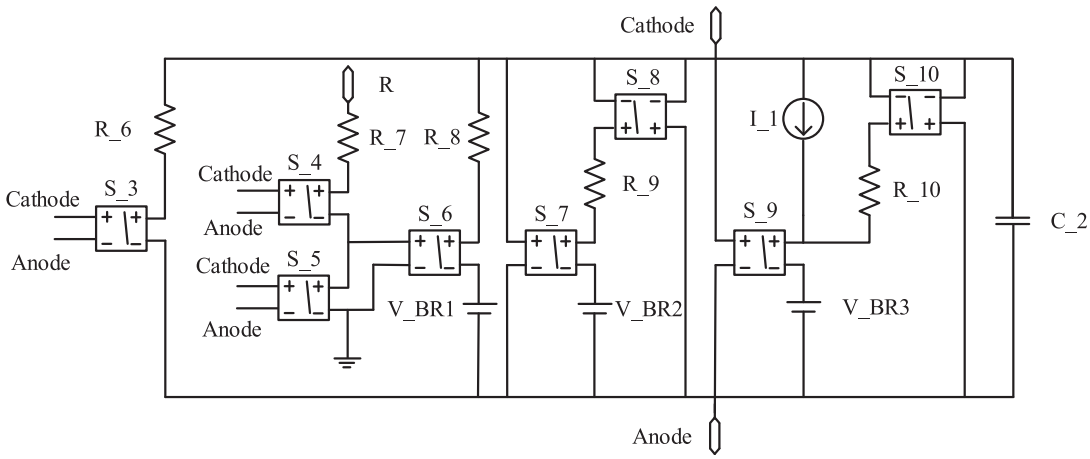

Fig. 7. Equivalent circuit model with RTS noise for SPAD devices.

current, which is used to simulate the avalanche current of the device. When the reverse bias voltage is less than the threshold voltage of the switch S_2, the switch S_2 is closed and the switch S_TRIG is open. At the same time, I_SELF is opened and the model has no current output. The input signal "Photon" is used to simulate photons, and the excitation source is a short positive pulse. When the reverse bias is greater than the threshold voltage of switch S_2, switch S_2 is open. If the input signal ' Photon ' is greater than the threshold voltage of the switch S_TRIG, the switch S_TRIG is closed. The current increases sharply, thus exceeding the threshold current of I_SELF. At this time, the output current of I_SELF is self-sustaining. Avalanche current is quenched only when the current of I_SELF is less than its threshold current. This requires a quench circuit. However, when the device is biased near its breakdown voltage, the avalanche current is not self-sustaining, it is self-quenching. Unfortunately, this behavior is not included in this model.

In this paper, an equivalent circuit model with RTS noise is implemented based on the equivalent circuit models shown in Figs. 5 and 6. This model is shown in Fig. 7. The model is built using basic components in Cadence. Therefore, it has strong application universality and is suitable for various simulation environments. This is very important for designers. When the reverse bias voltage is less than V_BR1, the device works in the linear region, and the switch S_3 is closed. The current in the linear region is very small. Therefore, the equivalent resistance R_6 in the linear region is very large. When the device is biased near its breakdown voltage, the switch S_5 is open and the switch S_4 is closed. The input signal "R" is used to simulate RTS noise and the excitation source is a short positive pulse. When the input signal "R" is greater than the threshold voltage of the switch S_6, the switch S_6 is closed, and the device generates an avalanche current. When the input signal "R" is less than the threshold voltage of the switch S_6, the switch S_6 is open and the avalanche current of the device self-quenches. The avalanche current is controlled by the input signal "R", which switches between the "ON" state and the "OFF" state. The equivalent resistances R_8 and R_9 of the SPAD device are mainly composed of the resistance of the space charge and the resistance of the neutral region.

When the reverse bias voltage is greater than V_BR2, the switches S_4, S_5, S_7 and S_8 are closed, and the switch S_6 is open. Resistor R_7 is used to prevent the input signal "R" from being directly grounded. When the reverse bias voltage increases, the avalanche current increases sharply. This is the steep phase in the IV curve. At this time, the avalanche current of the SPAD device is large and it will not self-quench. When the reverse bias voltage is greater than V_BR3, the switches S_8 and S_10 are open and the switch S_9 is closed. The avalanche current of the device tends to saturate. In this model, the constant current source I_1 is used to simulate the saturation current of the device. When the reverse bias voltage is less than V_BR3, switch S_9 is opened. At this time, if there is no resistor R_10 and switch S_10, the constant current source I_1 has no discharge path. This may cause the simulator to not converge. Therefore, when the reverse bias voltage is less than V_BR3, resistor R_10 and switch S_10 are used to provide a discharge path for I_1. It has no effect on the model. The values of resistor R_7 and resistor R_10 are not very important for this equivalent circuit model. In this paper, the resistance R_7 and resistance R_10 are set to 10 kΩ, and the simulation results and convergence of the model are satisfactory. C_2 is the equivalent capacitance of the device. It is worth noting that the threshold voltages of switches S_8 and S_10 are negative. This means that switches S_8 and S_10 are closed when the forward voltage is less than the threshold voltage.

IV. Experimental Results and Discussion

The test platform of RTS noise is shown in Fig. 8(a)–(c). The output voltage of the DC regulated power supply is 0 V to 30 V. The cathode of the device is connected with high voltage, and the anode is connected with sampling resistance R_11 (50 Ω). The sampling resistance R_11 is much smaller than the quenching resistance in Geiger mode (about 50 kΩ). The avalanche current of the device is converted into a voltage signal by the sampling resistor R_11. However, the voltage signal is very

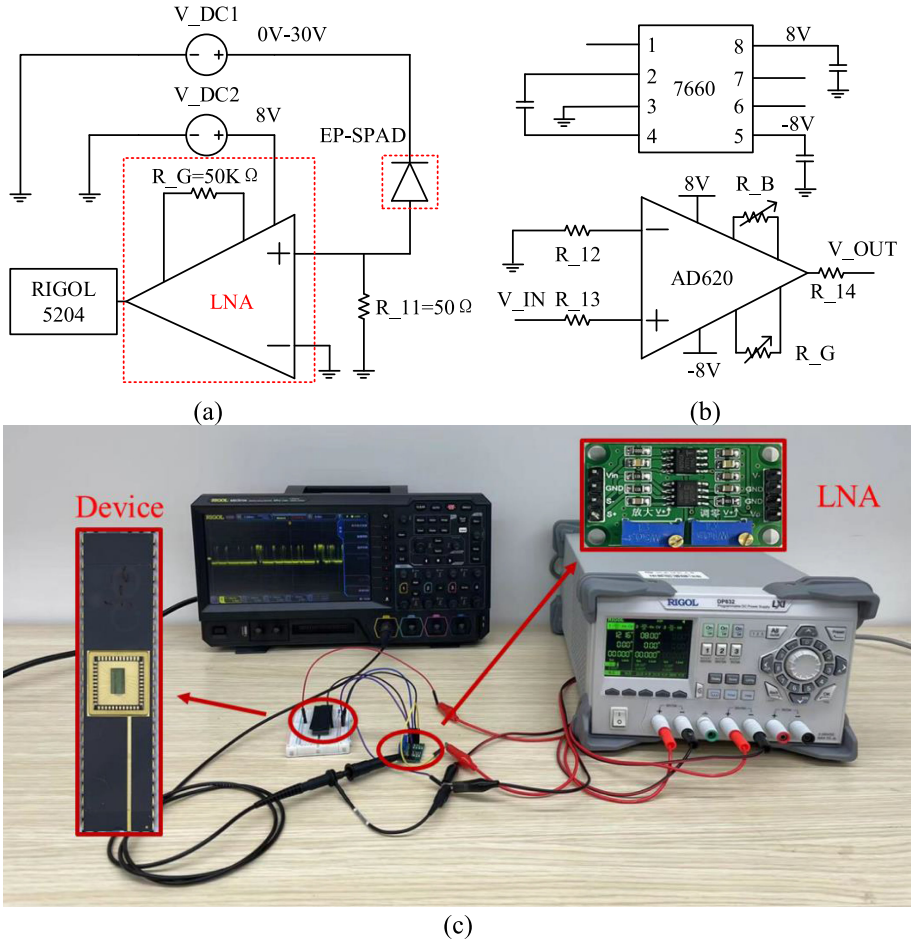

Fig. 8. (a) Test circuit for RTS noise. (b) The schematic diagram of the low noise amplifier circuit. (c) The test platform of the RTS noise.

small. Therefore, the voltage signal is amplified by a low noise amplifier (LNA) circuit. The LNA circuit is designed based on an instrumentation amplifier chip (AD620). The power supply voltage of AD620 is set to ± 8 V. The ICL7660 converts +8 V to −8 V. The resistor R_G is used to adjust the gain of the circuit. The resistor R_B is used to adjust the DC voltage of the circuit. Resistors R_12 and R_13 are input protection resistors for the AD620. Resistor R_14 is the output protection resistor for the AD620. They are set to 10 kΩ. The output V_OUT is connected to a high performance oscilloscope. Real-time acquisition of RTS noise at different reverse bias voltages. The collection time is 2 s. The test environment is dark.

Before testing RTS noise, we must know the avalanche breakdown voltage of the device. The IV characteristics of EP-SPAD devices were tested based on the B1505A system. The test results show that the avalanche breakdown voltage of the EP-SPAD device is 12.05 V. Therefore, in Fig. 8(a), the output voltage of V_DC1 is first set to 12.05 V. Then, the output voltage of V_DC1 is slowly increased, and the data in the oscilloscope is saved in real time. When the reverse bias voltage is less than 12.15 V, no RTS noise is observed in the EP-SPAD device. When the reverse bias voltage increases, the electric field in avalanche multiplication region increases sharply. This means that the avalanche probability of the device is increased. In addition, the avalanche current of the device also increases. When the reverse bias voltage of the device is 12.18V, the avalanche current of the EP-SPAD device is self-sustaining. The RTS noises under different reverse bias voltages are shown in Fig. 9(a)–(e), respectively. It can be seen from Fig. 9(b) and (c) that the avalanche probability of the EP-SPAD device is random. The avalanche current of the device is not self-sustaining. It is self-quenching. Therefore, the avalanche current always switches randomly between the "ON" state and the "OFF" state. This shows the behavior of RTS noise. As defined in [16], [17], [18], RTS noise is quantified by three parameters:

1) I_RTS, the current of RTS noise. It is the avalanche current of EP-SPAD device in the avalanche transition phase.
2) T_ON, which is the time the RTS noise is in the "ON" state.
3) T_OFF, which is the time the RTS noise is in the "OFF" state.

In this paper, the amplitude of the avalanche current is statistically analyzed based on the MATLAB platform. The statistical histograms of avalanche currents under different reverse bias voltages are shown in Fig. 10(a)–(e), respectively. There are two peaks in the L region of Fig. 10(c), the M region of 10(d),

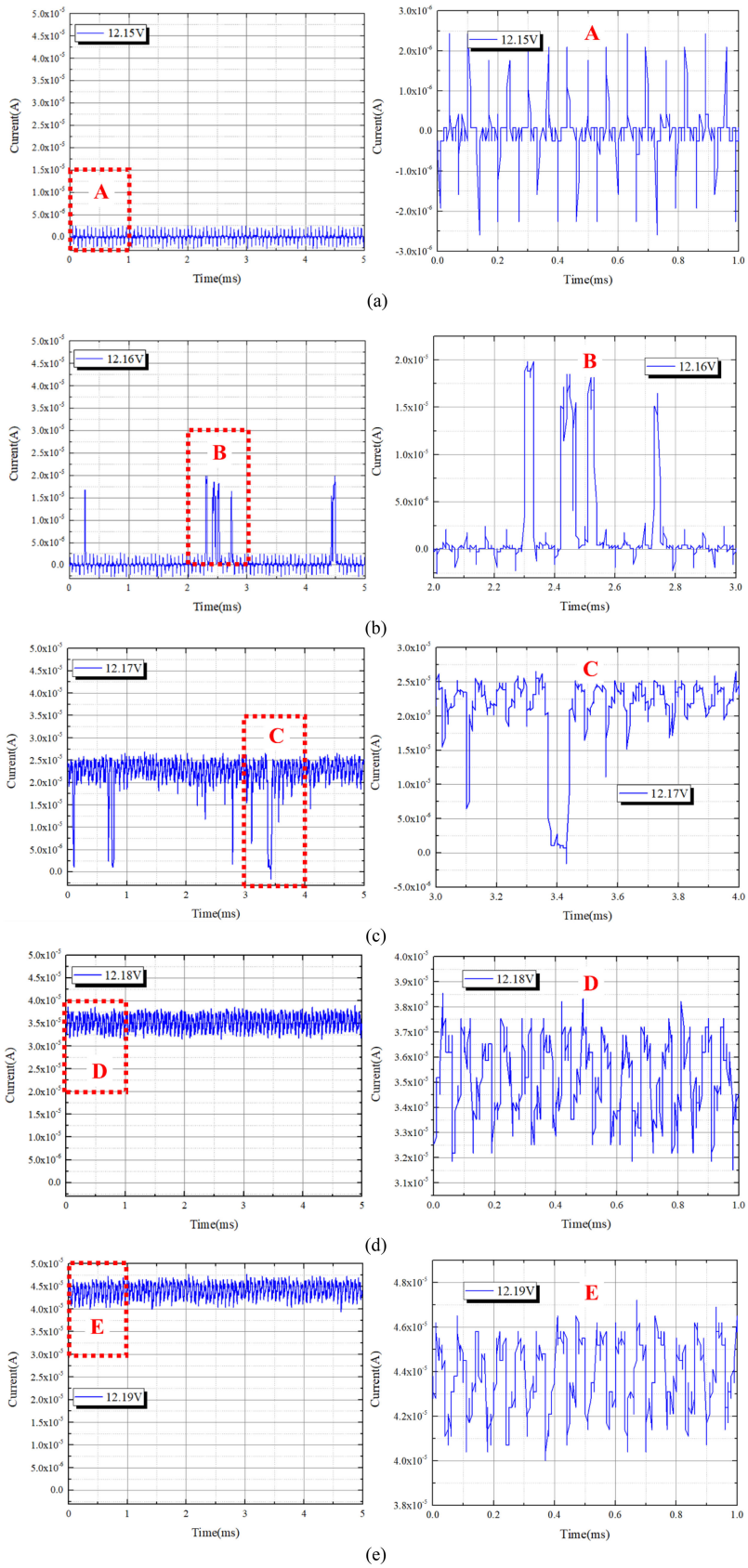

Fig. 9. (a) Current at 12.15 V. (b) Current at 12.16 V. (c) Current at 12.17 V. (d) Current at 12.18 V. (e) Current at 12.19 V.

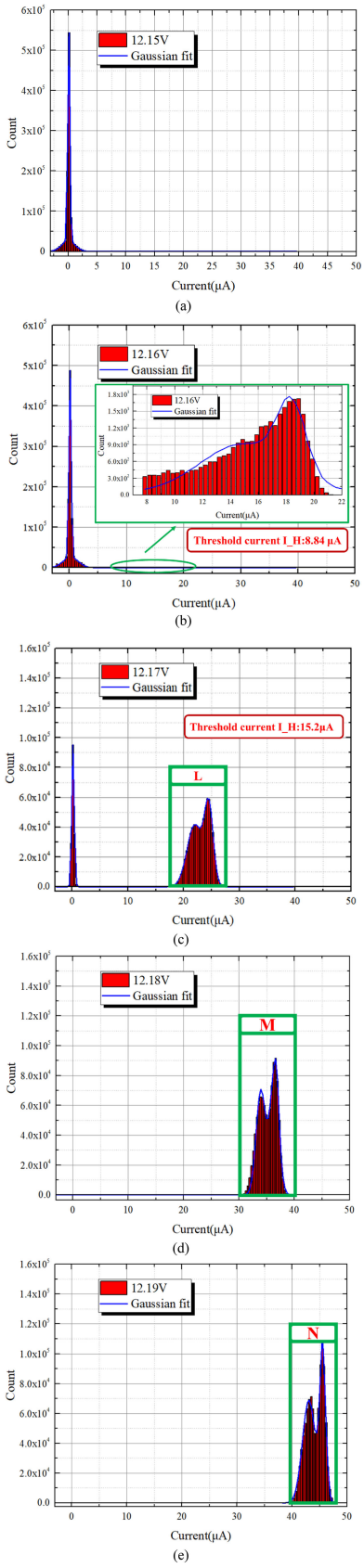

Fig. 10. (a) Current statistics at 12.15 V. (b) Current statistics at 12.16 V. (c) Current statistics at 12.17 V. (d) Current statistics at 12.18 V. (e) Current statistics at 12.19 V.

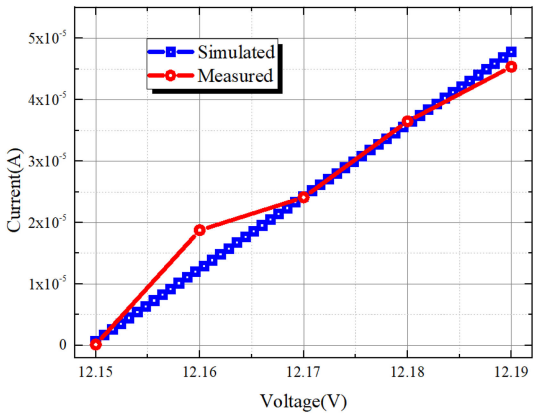

Fig. 11. The relationship between RTS noise current and reverse bias voltage.

and the N region of 10(e), which are mainly caused by random noise in the test circuit. For example, in Fig. 10(d), there are two peaks in region M. Random noise in the test circuit causes the avalanche current to not be a constant value. The avalanche current varies from 3.15×10^{-5} A to 3.75×10^{-5} A, as shown in Fig. 9(d). Therefore, there are two peaks in region M. In theory, there is only one peak in region M. However, this has less impact on the test results. Because the average value of the avalanche current is finally obtained by Gaussian fitting.

The relationship between the current average value and the reverse bias voltage is shown in Fig. 11. The current of the EP-SPAD device is 0.144 μA at 12.15 V. As the reverse bias voltage increases, the probability of impact ionization of carriers increases, resulting in an increase in the number of carriers. Therefore, the avalanche current reaches 45.4 μA at 12.19 V. The equivalent resistance R_8 in the model can be calculated from (1).

$$\mathrm{R\_8} = \frac{\Delta V}{\Delta I} = \frac{12.19\,V - 12.15\,V}{45.4\,\mu A - 0.1445\,\mu A} = 884\Omega \qquad (1)$$

When the equivalent resistance R_8 is set to 850 Ω, the model has higher accuracy. The simulation results of the RTS noise current are shown in Fig. 11.

In Fig. 10, the current threshold I_H is set to calculate the T_ON and T_OFF of the RTS noise. For example, when the reverse bias voltage is 12.17 V, the current threshold I_H is set to 15.2 μA. When the current is less than 15.2 μA, the avalanche current is considered to be off. When the current is greater than 15.2 μA, the avalanche current is considered to be on. The dependence of T_ON and T_OFF on reverse bias voltage is shown in Fig. 12. The electric field strength increases with the reverse bias voltage. Dark carriers in the depletion region are more likely to trigger avalanche currents. This means that the avalanche current is more likely to stay in the "ON" state rather than the "OFF" state. Therefore, as the reverse bias voltage increases, T_ON increases and T_OFF decreases. As defined in [16], [17], [18], the duty cycle of the RTS noise can be calculated

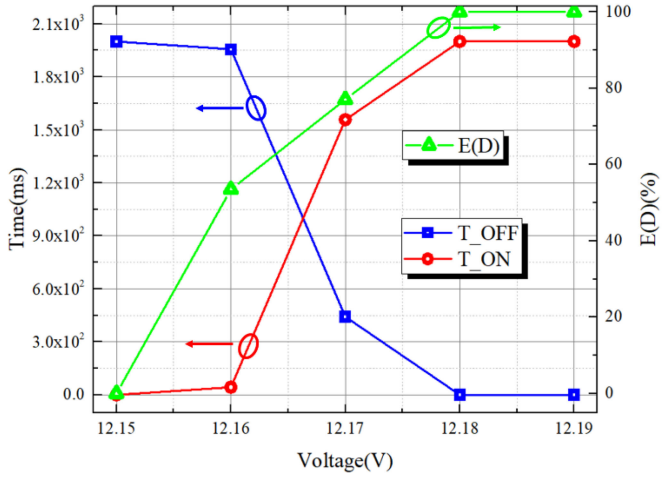

Fig. 12. Dependence of T_ON, E(D) and T_OFF on reverse bias voltage.

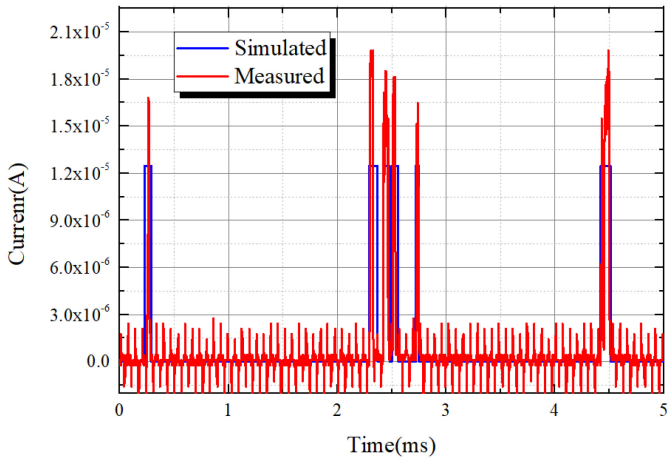

Fig. 13. Simulation waveform and test waveform of RTS noise at 12.16 V.

from (2).

$$E\ (D) = \frac{T\_ON}{T\_ON + T\_OFF} \times 100\% \tag{2}$$

The duty cycle of RTS noise is shown in Fig. 12. The duty cycle E(D) of RTS noise increases with the increase of reverse bias voltage. When the reverse bias voltage is 12.18 V, the T_ON is 2 s and the duty cycle is 100%. The avalanche current of the EP-SPAD device is 36.5 μA. At this time, the avalanche current of the EP-SPAD device is self-sustaining. The EP-SPAD device enters stable Geiger mode. It is well known that in the field of weak light detection, it is very important for SPAD devices to work in stable Geiger mode. However, the threshold voltage of the Geiger mode is not precisely defined in many works. In this paper, the threshold voltage of the EP-SPAD device operating in Geiger mode is 12.18V. If the reverse bias voltage is less than 12.18 V, the avalanche current of the device is unstable, which can cause false counts in the signal processing circuit. In this paper, the parameters of the input signal "R" are set based on the actual waveform of the RTS noise. It is very easy to realize by the relevant timing generation circuit. The simulated waveform of RTS noise is shown in Fig. 13.

The IV curve of the EP-SPAD device is shown in Fig. 14. It is tested based on the B1505A system. The cathode voltage of the EP-SPAD device is set to increase from 0 V to 15 V and the anode voltage is set to 0 V. The test environment is dark. The avalanche breakdown voltage of the EP-SPAD device is 12.05 V. If 2 V $\leq$ V_R $\leq$ 12.05 V, the EP-SPAD device operates in the linear region. The current in the linear region of the EP-SPAD device is 10^{-11} A. The equivalent resistance R_6 in the linear region can be calculated from (3).

$$\mathrm{R\_6} = \frac{\Delta V}{\Delta I} = \frac{12.05V - 2V}{6.5 \times 10^{-11}A - 5.4 \times 10^{-13}A} = 156G\Omega \tag{3}$$

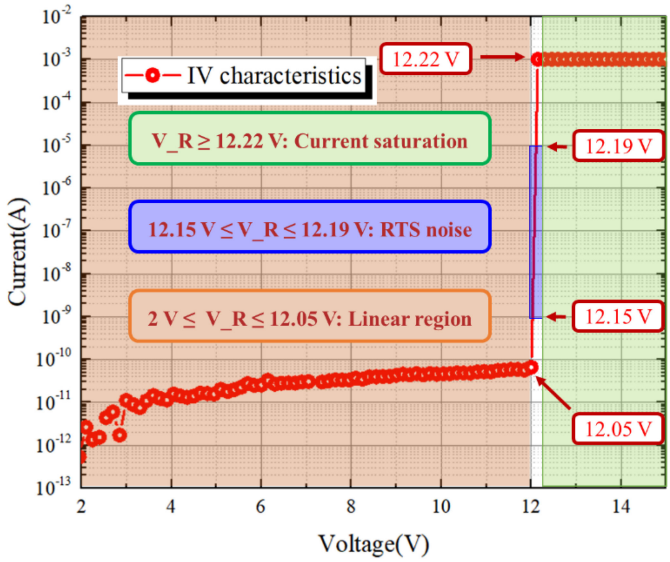

Fig. 14. IV characteristics of the EP-SPAD device.

When the reverse bias voltage is greater than 12.15 V, RTS noise begins to appear in the EP-SPAD device. When the reverse bias voltage is 12.19 V, the RTS noise has completely disappeared, and the avalanche current of the EP-SPAD device is 45.4 μA. When the reverse bias voltage is greater than 12.22 V, the avalanche current of the EP-SPAD device tends to be saturated. The saturation current of the EP-SPAD device is 1 mA. Therefore, the current gain of the EP-SPAD device is 10^8. The equivalent resistance R_9 can be calculated from (4).

$$R\_9 = \frac{\Delta V}{\Delta I} = \frac{12.22\,V - 12.19\,V}{1000\,\mu A - 45.4\,\mu A} = 31.43\,\Omega \tag{4}$$

The equivalent resistance R_9 is set to 30.6 Ω, the model has high accuracy.

The simulated IV curve is shown in Fig. 15, which is consistent with the test results. In conclusion, this equivalent circuit model can accurately characterize the IV characteristics of the

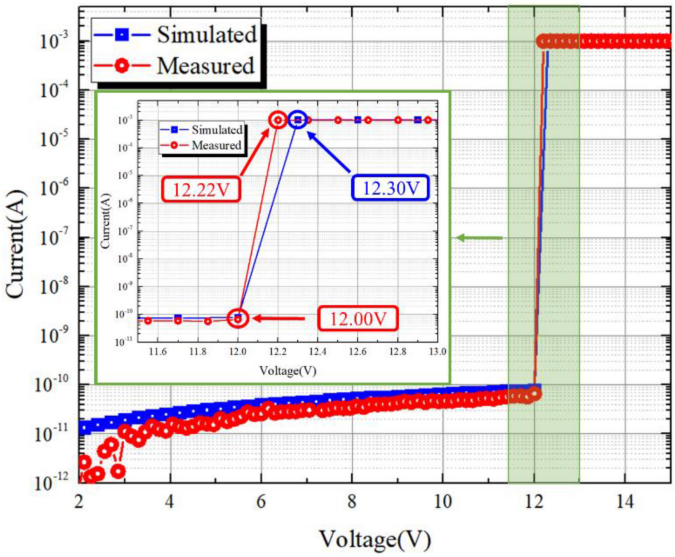

Fig. 15. IV characteristics of the equivalent circuit model.

TABLE I
PARAMETERS OF COMPONENTS IN THE EQUIVALENT CIRCUIT MODEL

Components	Value
R_6	156 GΩ
R_7	10 kΩ
R_8	850 Ω
R_9	30.6 Ω
R_10	10 kΩ
VBR_1	12.149 V
VBR_2	12.189 V
VBR_3	12.22 V
I_1	1 mA

EP-SPAD device, and it contains RTS noise. The RTS noise is included in the equivalent circuit model of the SPAD device, which makes the model more complete and accurate. The equivalent capacitance of the device is not analyzed and modeled in this paper. For example, the equivalent capacitance C_2 between the cathode and the anode, the equivalent capacitance C_CS between the cathode and the substrate, and the equivalent capacitance C_AS between the anode and the substrate. Therefore, it cannot simulate the timing behavior of SPAD devices at present. In order to simulate the timing behavior, the equivalent capacitance in the SPAD device needs to be analyzed and modeled. In Fig. 7, the parameters of the equivalent circuit model are shown in Table I.

V. CONCLUSION

In this paper, the RTS noise of EP-SPAD device is tested and analyzed, and the equivalent circuit model with RTS noise is realized based on Cadence. It is fully compatible with other commercial circuit simulators. The model includes the self-sustaining and self-quenching behavior of avalanche currents in SPAD devices, and its convergence is satisfactory. To the best of our knowledge, this is the first time that RTS noise has been included in the equivalent circuit model. The model is validated in a novel embedded photogate SPAD device, and the process of extracting model parameters based on test data is shown. The dependence of the RTS noise on the reverse bias voltage in the simulation is consistent with the test. The maximum error between the simulation current and the test current is about 5.74uA. The threshold voltage of the EP-SPAD device operating in Geiger mode is given based on the RTS noise characteristics. When the reverse bias voltage of the device is increased from 0 V to 15 V, the model can accurately characterize the IV characteristics of the EP-SPAD device, and the simulation results are satisfactory.

REFERENCES

[1] F. Ceccarelli, G. Acconcia, A. Gulinatti, M. Ghioni, I. Rech, and R. Osellame, "Recent advances and future perspectives of single-photon avalanche diodes for quantum photonics applications," *Adv. Quantum Technol.*, vol. 4, no. 2, 2021, Art. no. 2000102.

[2] I. Takai, H. Matsubara, M. Soga, M. Ohta, M. Ogawa, and T. Yamashita, "Single-photon avalanche diode with enhanced NIR-sensitivity for automotive LIDAR systems," *Sensors*, vol. 16, no. 4, 2016, Art. no. 459.

[3] N. Faramarzpour, M. J. Deen, S. Shirani, and Q. Fang,, "Fully integrated single photon avalanche diode detector in standard CMOS 0.18 μm technology," *IEEE Trans. Electron Devices*, vol. 55, no. 3, pp. 760–767, Mar. 2008.

[4] A. Dervić, M. Hofbauer, B. Goll, and H. Zimmermann, "Integrated fast-sensing triple-voltage SPAD quenching/resetting circuit for increasing PDP," *IEEE Photon. Technol. Lett.*, vol. 33, no. 3, pp. 139–142, Feb. 2021.

[5] Z. Cheng, D. Palubiak, X. Zheng, M. J. Deen, and H. Peng, "Impact of silicide layer on single photon avalanche diodes in a 130 nm CMOS process," *J. Phys. D: Appl. Phys.*, vol. 49, no. 34, 2016, Art. no. 345105.

[6] R. Mita, G. Palumbo, and P. G. Fallica, "Accurate model for single-photon avalanche diodes," *IET Circuits, Devices Syst.*, vol. 2, no. 2, pp. 207–212, 2008.

[7] D. P. Palubiak, Z. Li, and M. J. Deen, "Afterpulsing characteristics of free-running and time-gated single-photon avalanche diodes in 130-nm CMOS," *IEEE Trans. Electron Devices*, vol. 62, no. 11, pp. 3727–3733, Nov. 2015.

[8] G. Giustolisi, R. Mita, and G. Palumbo, "Behavioral modeling of statistical phenomena of single-photon avalanche diodes," *Int. J. Circuit Theory Appl.*, vol. 40, no. 7, pp. 661–679, 2012.

[9] Z. Cheng, X. Zheng, D. Palubiak, M. J. Deen, and H. Peng, "A comprehensive and accurate analytical SPAD model for circuit simulation," *IEEE Trans. Electron Devices*, vol. 63, no. 5, pp. 1940–1948, May 2016.

[10] A. Gulinatti, I. Rech, M. Assanelli, M. Ghioni, and S. Cova, "A physically based model for evaluating the photon detection efficiency and the temporal response of SPAD detectors," *J. Modern Opt.*, vol. 58, no. 3/4, pp. 210–224, 2011.

[11] L. Pancheri, D. Stoppa, and G.-F. D. Betta, "Characterization and modeling of breakdown probability in sub-micrometer CMOS SPADs," *IEEE J. Sel. Topics Quantum Electron.*, vol. 20, no. 6, pp. 328–335, Nov./Dec. 2014.

[12] V. Savuskan, I. Brouk, M. Javitt, and Y. Nemirovsky, "An estimation of single photon avalanche diode (SPAD) photon detection efficiency (PDE) nonuniformity," *IEEE Sensors J.*, vol. 13, no. 5, pp. 1637–1640, May 2013.

[13] S. Tisa, F. Zappa, A. Tosi, and S. Cova, "Electronics for single photon avalanche diode arrays," *Sensors Actuators A: Phys.*, vol. 140, no. 1, pp. 113–122, 2007.

[14] A. Dalla Mora, A. Tosi, S. Tisa, and F. Zappa, "Single-photon avalanche diode model for circuit simulations," *IEEE Photon. Technol. Lett.*, vol. 19, no. 23, pp. 1922–1924, Dec. 2007.

[15] F. Zappa, A. Tosi, A. D. Mora, and S. Tisa, "SPICE modeling of single photon avalanche diodes," *Sensors Actuators A: Phys.*, vol. 153, no. 2, pp. 197–204, 2009.

[16] V. Agarwal, A. -J. Annema, S. Dutta, R. J. E. Hueting, L. K. Nanver, and B. Nauta, "Random telegraph signal phenomena in ultra shallow p^+ n silicon avalanche diodes," *IEEE J. Electron Devices Soc.*, vol. 6, pp. 642–652, 2018.

[17] W. Jiang and M. J. Deen, "Random telegraph signal in n^+/p-well CMOS single-photon avalanche diodes," *IEEE Trans. Electron Devices*, vol. 68, no. 6, pp. 2764–2769, Jun. 2021.

[18] V. Agarwal, A. J. Annema, S. Dutta, R. J. E. Hueting, L. K. Nanver, and B. Nauta, "Random telegraph signal phenomena in avalanche mode diodes: Application to SPADs," in *Proc. 46th Eur. Solid-State Device Res. Conf.*, 2016, pp. 264–267.

[19] F. D. Capua et al., "Random telegraph signal in proton irradiated single-photon avalanche diodes," *IEEE Trans. Nucl. Sci.*, vol. 65, no. 8, pp. 1654–1660, Aug. 2018.

[20] M. A. Karami, L. Carrara, C. Niclass, M. Fishburn, and E. Charbon, "RTS noise characterization in single-photon avalanche diodes," *IEEE Electron Device Lett.*, vol. 31, no. 7, pp. 692–694, Jul. 2010.

[21] C. Chen, X. Jin, and J. Luo, "A novel composite UV/blue photodetector based on CMOS technology: Design and simulation," *Optoelectron. Lett.*, vol. 9, no. 6, pp. 414–417, 2013.

[22] J. A. Richardson, L. A. Grant, and R. K. Henderson, "Low dark count single-photon avalanche diode structure compatible with standard nanometer scale CMOS technology," *IEEE Photon. Technol. Lett.*, vol. 21, no. 14, pp. 1020–1022, Jul. 2009.

[23] T. Leitner et al., "Measurements and simulations of low dark count rate single photon avalanche diode device in a low voltage 180-nm CMOS image sensor technology," *IEEE Trans. Electron Devices*, vol. 60, no. 6, pp. 1982–1988, Jun. 2013.

[24] M. M. Vignetti, F. Calmon, R. Cellier, P. Pittet, L. Quiquerez, and A. Savoy-Navarro, "Design guidelines for the integration of Geiger-mode avalanche diodes in standard CMOS technologies," *Microelectronics J.*, vol. 46, no. 10, pp. 900–910, 2015.